



# Experimental study on the effect of pyrolysis temperature on the NO emission and conversion during combustion

Yuan Xiao<sup>1,2</sup> · Guoliang Song<sup>1,2,3</sup> · Qinggang Lyu<sup>1,2,3</sup>

Received: 19 March 2020 / Accepted: 16 July 2020 / Published online: 30 July 2020  
© Akadémiai Kiadó, Budapest, Hungary 2020

## Abstract

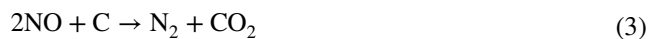
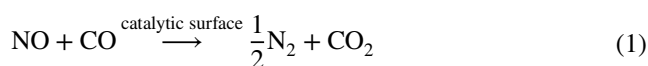
For realizing the coupling pyrolysis of coal and combustion of semi-coke, this paper explored the effect of pyrolysis temperature on the combustion characteristics and NO emission of Pingshuo semi-coke. The main physical and chemical properties, which might affect the NO emission, were also investigated systematically. As the pyrolysis temperature increased, the nitrogen content of semi-coke gradually decreased and the proportion of quaternary nitrogen (N-Q) gradually increased. CaO produced by the decomposition of CaCO<sub>3</sub> would promote the transformation from HCN to NO. Pore structure was most developed at 750 °C, which was beneficial to the conversion of HCN and reduction of NO. Combustion experiments were carried out on a thermogravimetric–mass spectrometry. It was found that increasing the pyrolysis temperature would cause the combustion reaction to occur at a higher temperature. Evolved gases during the combustion were quantitatively analyzed by equivalent characteristic spectrum analysis. The yield of HCN during combustion first decreased and then increased and the yield of NO decreased while the pyrolysis temperature increased. There was an optimum pyrolysis temperature for the minimum conversion rate of fuel-N to NO and HCN. For Pingshuo bituminous, this optimum pyrolysis temperature was 750 °C.

**Keywords** Pingshuo semi-coke · Pyrolysis temperature · Combustion · HCN · NO

## Introduction

Coal is dominant in China's energy consumption structure. Though coal takes up a year-on-year decline in the proportion of China's total energy consumption, its absolute consumption is yet at a relatively stable level, and it will remain in the near future [1]. The cascade utilization of coal is regarded as a kind of promising technology to use low-rank coal. The cascade utilization of coal is divided into two steps. Firstly, the coal pyrolysis, and part of the volatile matter in the coal will be released in the form of pyrolysis gas and tar. Next, the semi-coke is combusted in thermal power plants [2]. NO<sub>x</sub> is inevitably produced during the combustion of coal. Many studies have proved that the NO emission

was determined by the generation rate of char-N to NO and the reduction rate of NO [3, 4]. The NO reduction reactions mainly contain homogeneous reduction and heterogeneous reduction [5, 6], which are listed in the following:



The catalytic surface in a homogeneous surface mainly refers to the char surface. Therefore, both homogeneous reduction and heterogeneous reduction depend on the reactivity and structure of char [7–10]. In addition, many scholars have proved that alkali and alkaline earth metals can influence the generation of NO<sub>x</sub> precursors during pyrolysis and release of NO<sub>x</sub> in combustion [11–17]. Total nitrogen content is considered the most important factor to influence the generation of NO during combustion [18]. Pyrolysis temperature can significantly affect the above factors, which affect NO<sub>x</sub> emission. Therefore, it is crucial to find an

✉ Guoliang Song  
songgl@iet.cn

<sup>1</sup> Institute of Engineering Thermalphysics, Chinese Academy of Sciences, Beijing 100190, China

<sup>2</sup> University of Chinese Academy of Sciences, Beijing 100049, China

<sup>3</sup> Dalian National Laboratory for Clean Energy, Dalian 116023, China

**Table 1** Analysis of PS and its semi-coke/%

Sample	Proximate analysis				Ultimate analysis				
	M <sub>ar</sub>	A <sub>ar</sub>	V <sub>ar</sub>	FC <sub>ar</sub>	C <sub>ar</sub>	H <sub>ar</sub>	O <sub>ar</sub>	N <sub>ar</sub>	S <sub>ar</sub>
PS	2.20	54.64	21.02	22.14	29.26	2.51	8.46	1.10	2.44

The subscript “ar” meant “As received”

**Table 2** Ash composition of PS/%

Items	SiO <sub>2</sub>	Al <sub>2</sub> O <sub>3</sub>	CaO	SO <sub>3</sub>	Fe <sub>2</sub> O <sub>3</sub>	TiO <sub>2</sub>	K <sub>2</sub> O	MgO	P <sub>2</sub> O <sub>5</sub>	Na <sub>2</sub> O
PS	47.55	34.39	5.60	5.08	3.97	1.67	0.62	0.59	0.17	0.08

optimum pyrolysis temperature to minimize the emission of NO and its precursor for semi-coke.

Existing studies focus on the influences of pyrolysis conditions on NO<sub>x</sub> precursors [19–22] or the influences of combustion conditions on NO<sub>x</sub> formation [23–29]. In this study, the pyrolysis and the combustion were regarded as a continuous process to investigate the effect of pyrolysis temperature on semi-coke combustion. Furthermore, the effect of pyrolysis temperature on the factors affecting NO<sub>x</sub> emissions, such as nitrogen content, pore structure and mineral composition, was systematically explored. Combustion characteristics of semi-coke at different pyrolysis temperatures were investigated on TG–MS. For the quantitative analysis of the evolved gas during the combustion, equivalent characteristic spectrum analysis (ECSA) was used [30–32]. The yield of HCN and NO was calculated; hence, the influence of pyrolysis temperature on the conversion rate of HCN and NO was obtained.

## Experimental

### Materials

The test coal Pingshuo bituminous (PS) was produced by the Antaibao Open-pit Coal Mine in Pingshuo, Shanxi province. Coal was crushed and then sieved to a particle size between 0 and 0.2 mm. The proximate and ultimate analysis of PS was performed. The results are shown in Table 1.

An ash composition analysis of PS was performed. The analysis results are listed in Table 2. It was obvious that the ash in the samples was dominated by SiO<sub>2</sub> and Al<sub>2</sub>O<sub>3</sub>.

### Apparatus

The pyrolysis experiments of Pingshuo bituminous were performed in a high temperature and high flux horizontal quartz tube furnace reactor. The model of this reactor was SK-G08143, as shown in Fig. 1.

Dimensions of the device were 400 mm × 614 mm × 653 mm. The major body of the reactor

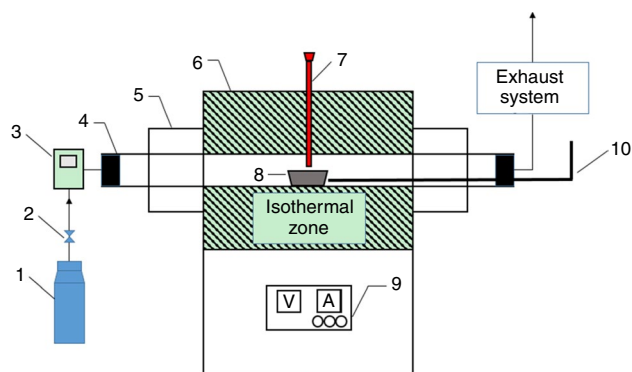


**Fig. 1** Horizontal quartz tube furnace reactor. 1 Gas cylinder; 2 pressure-reducing valve; 3 gas flow meter; 4 reactor; 5 support; 6 electric furnace; 7 thermocouple; 8 corundum boat; 9 temperature controller; 10 putter

system was a corundum tube that exhibited an inner diameter of 70 mm and a length of 1000 mm. The maximum temperature the corundum tube could withstand was 1400 °C. The electric furnace exhibited a rated power of 5 kW, the heating element was a carbon-silicon rod, and the constant temperature zone had a length of 150 mm. Besides, the temperature control system consisted of a thermocouple and a temperature controller. The carrier gas system was composed of a gas cylinder, a pressure-reducing valve, as well as a gas flow meter.

To explore the NO emission characteristics of Pingshuo semi-coke accurately, the combustion experiments were carried out on a TG–MS system. The TG–MS system employed in this study consisted of the STA449F3 thermogravimetric analyzer from Germany NETZSCH and the QMS403C Aeolosquadrupole mass spectrometer. The system was capable of monitoring the formation of various gases online.

### Experimental methods

**Pyrolysis experiment:** To better simulate the pyrolysis process in the actual production process, the rapid pyrolysis process rather than the program heating pyrolysis process was used for this experiment. First, the horizontal tube

furnace was set to the specified temperature (600, 750, 900 °C). Simultaneously, N<sub>2</sub> was purging to the reactor at a flow rate of 5 L/min. When the furnace was in an inert atmosphere, the coal sample (5 ± 0.1 g) was put into the isothermal zone of the pyrolysis reactor in a corundum boat (150\*50\*20 mm). In order to ensure that the samples could get devolatilization sufficiently, each condition would remain for 15 min. Tar and pyrolysis gas were emptied to the exhaust system. At the end of each condition, the furnace was turned off, and N<sub>2</sub> was kept purging to maintain the inert atmosphere until the semi-coke sample was cooled to ambient temperature. Then, the sample was taken out and stored.

**Combustion experiment:** The combustion experiments were performed on a TG–MS system, in order to explore the combustion and NO emission characteristics accurately. Moreover, 30 mg of the sample was put into the thermogravimeter with a crucible for each condition. After purging and desorption process, the combustion experiments were carried out with a gas flow of 65 mL min<sup>-1</sup> Ar and 5 mL min<sup>-1</sup> O<sub>2</sub>. The samples were heated from ambient temperature to 1200 °C at the heating rate of 10 °C min<sup>-1</sup>. The selection of the above parameters was based on previous experience [32]. The reason for selecting the above experiment parameters was to control an appropriate combustion rate. A too high combustion rate could cause inaccurate analysis. The gas pollutant from the TG entered the MS through a heated stainless steel capillary. The quantitative analysis of the evolved gas was calculated by ECSA [30–32].

## Results and discussion

### Physical and chemical properties of samples

#### Nitrogen content of samples

During the process of pyrolysis, the organic nitrogen would release in the form of pyrolysis gas and tar. The content of nitrogen in coal was one of the most crucial factors, which would affect the NO emission. Therefore, the element analysis of semi-coke was carried out, and the results are shown in Fig. 2. For comparison, the elemental analysis results of Pingshuo bituminous are also shown in Fig. 2.

After pyrolysis, all element contents decreased, except C. Due to the release of volatile during pyrolysis, the content of O, H and N decreased. Corresponding, the fixed carbon content of semi-coke was higher than PS.

With the pyrolysis temperature increasing, the content of O, H and N decreased. However, the content of S showed an opposite trend. This was because tar contained more S than pyrolysis gas. Moreover, the tar was released at a relatively lower temperature, below 600 °C.

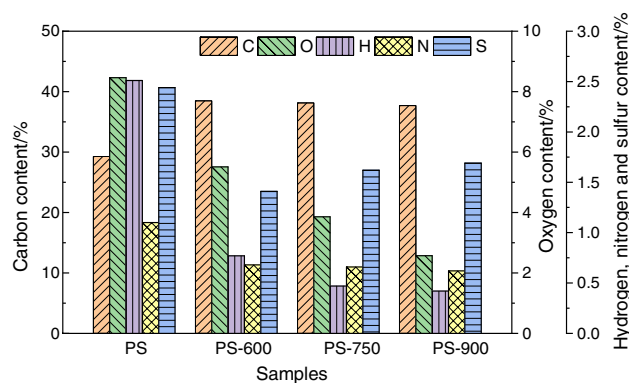


Fig. 2 Element analysis results of samples

Table 3 Binding energy of nitrogen morphology

Nitrogen morphology	Symbol	Binding energy/eV
Pyridine	N-6	398.7 ± 0.4
Pyrrole	N-5	400.5 ± 0.3
Quaternary nitrogen	N-Q	401.5 ± 0.3
Oxidized nitrogen	N-X	403.5 ± 0.3

Comparing the absolute nitrogen content in PS and its semi-coke, which is shown in Fig. 2, it was found that the release of nitrogen in the form of pyrolysis gas mainly occurred when the pyrolysis temperature was below 600 °C. The content of nitrogen in different semi-cokes was almost the same. When the pyrolysis temperature exceeded 600 °C, the transformation of different nitrogen compounds may occur mainly.

Therefore, the species of nitrogen morphology in PS and its semi-cokes were also investigated by XPS (THERMO, 250XI). According to existing studies, there were usually four species of nitrogen compounds in coal according to binding energy [33, 34]. Detailed classification is listed in Table 3.

The results of the curve fitting of XPS-N1s spectra for PS and its semi-coke are shown in Fig. 3. In Fig. 3, the ordinate and the abscissa represented the signal strength of the intensity and the binding energy, respectively. Four types of nitrogen morphology were identified by the binding energy.

Relative content of nitrogen compounds can be obtained from the area under the curve. Thus, the relative content of nitrogen morphology in all samples was obtained. The result is shown in Table 4.

The absolute content of different nitrogen morphology could be calculated by the absolute content of nitrogen and relative content of different nitrogen morphology. The calculated results are shown in Fig. 4.

A comparison of PS and PS-600 revealed that there was a reduction in contents of all nitrogen morphology after

**Fig. 3** Curve fitting of XPS-N1s spectra for PS and its semi-coke

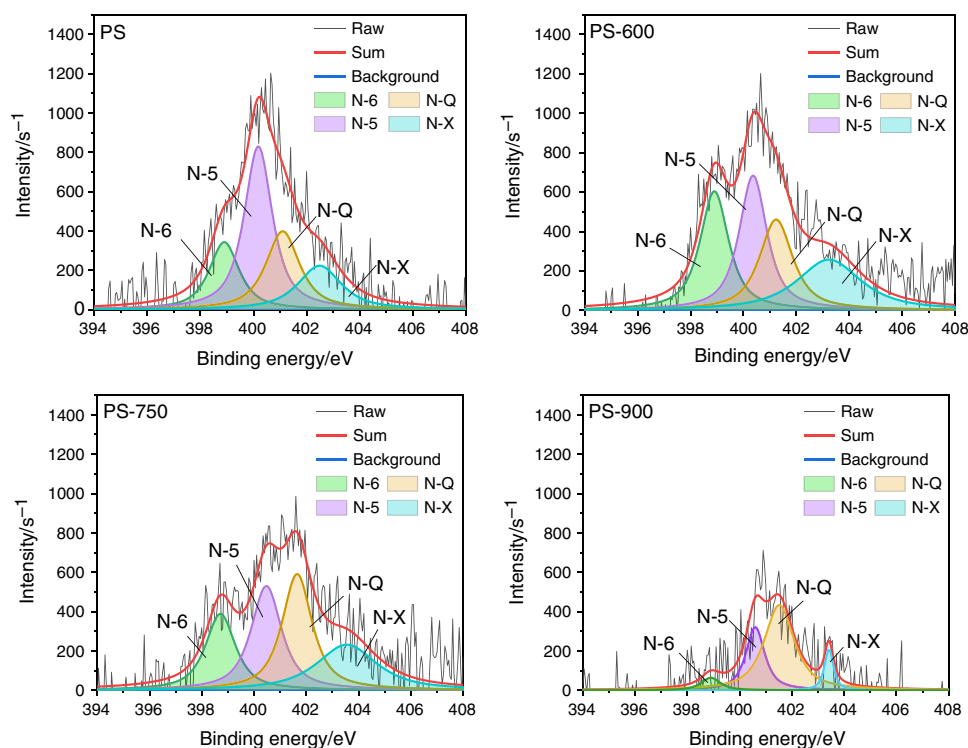


**Table 4** Relative content of nitrogen compounds in samples

Nitrogen morphology/%	PS	PS-600	PS-750	PS-900
N-6	18.16	25.39	19.57	5.59
N-5	41.03	27.89	27.09	27.28
N-Q	23.62	22.49	29.87	58.67
N-X	17.19	24.23	23.48	8.46

increased. In addition, N-5 was almost unchanged with the increase of pyrolysis temperature. When the pyrolysis temperature increased from 600 to 900 °C, N-6 and N-X decreased with different degrees. Especially, from 750 to 900 °C, there was an obvious drop of N-6 and N-X. With the rising temperature, the absolute content of N-Q increased while N-6 and N-X decreased in the semi-coke, indicating that N-6 and N-X transformed to N-Q. It was because that N-Q had the best thermal stability at high temperatures.

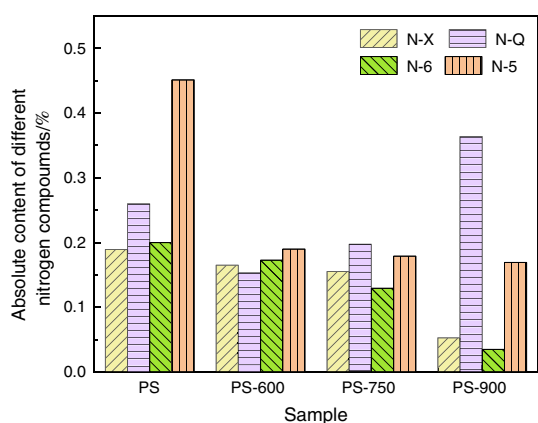


**Fig. 4** Absolute content of nitrogen morphology in samples

pyrolysis. Nevertheless, the decline in the content of N-Q and N-5 was more pronounced. With the pyrolysis temperature increasing, the absolute content of N-Q gradually

### Mineral compositions in samples

Different mineral compositions in coal had a different influence on the NO emission characteristics. Some minerals in coal may become a catalyst in the reduction reaction between char and NO. Some minerals could promote the coal combustion process. Besides, the decomposition of the mineral would affect the result of the TG/DTG analysis. Therefore, the mineral composition of samples must be investigated. In order to exclude the influence of fixed carbon and to ensure that the ash composition was not changed as much as possible, the low-temperature ashing method was used. After ashing, the ash compositions of samples were analyzed by XRF (Shimadzu, XRF-1800). The results are listed in Table 5. The main ash compositions of all samples were SiO<sub>2</sub> and Al<sub>2</sub>O<sub>3</sub>. The content of alkali metal was relatively low. Furthermore, there was almost no change in the content of the alkali metal.

**Table 5** Mineral compositions in samples

Items	SiO <sub>2</sub>	Al <sub>2</sub> O <sub>3</sub>	CaO	SO <sub>3</sub>	Fe <sub>2</sub> O <sub>3</sub>	TiO <sub>2</sub>	K <sub>2</sub> O	MgO	P <sub>2</sub> O <sub>5</sub>	Na <sub>2</sub> O
PS	47.55	34.39	5.60	5.08	3.97	1.67	0.62	0.59	0.17	0.08
PS-600	46.77	33.87	5.77	6.09	4.08	1.61	0.69	0.58	0.17	0.06
PS-750	47.11	33.86	4.98	6.74	3.95	1.67	0.62	0.54	0.20	0.07
PS-900	47.01	33.80	4.93	6.92	3.87	1.65	0.64	0.60	0.20	0.08

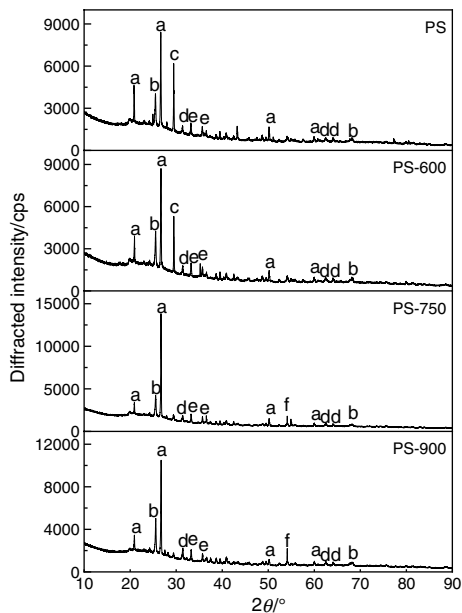


**Fig. 5** XRD pattern of PS and its semi-coke. a SiO<sub>2</sub>; b Al<sub>2</sub>O<sub>3</sub>; c CaCO<sub>3</sub>; d CaSO<sub>4</sub>; e Fe<sub>2</sub>O<sub>3</sub>; f CaO

The XRF could not analyze the specific compositions in samples. For this reason, the analysis of crystal phase composition was carried out on XRD (Rigaku, Smartlab 9). Figure 5 shows the analysis results of the XRD crystal phase composition in the samples.

The XRD results indicated that SiO<sub>2</sub> and Al<sub>2</sub>O<sub>3</sub> were abundant in the samples. The crystal phase compositions of Ca in samples were worth noting. There were CaCO<sub>3</sub> and CaSO<sub>4</sub> in PS and PS-600. However, CaCO<sub>3</sub> was not found in PS-750 and PS-900. A weaker peak of CaO was observed in PS-750, indicating CaCO<sub>3</sub> started to decompose at 750 °C. For PS-900, the intensity of the CaO peak increased, owing to more thoroughly decomposition reaction of CaCO<sub>3</sub>. The HCN and NO emission of PS-750 and PS-900 might be influenced by the presence of CaO.

**Morphological properties of semi-cokes**

The structure of the semi-coke was much different with coal. In addition, the structure of semi-coke was affected by pyrolysis temperature [35]. As above-mentioned, char could provide active sites for the NO reduction reaction,

**Table 6** Morphological properties of semi-coke

Sample	BET surface area/m <sup>2</sup> g <sup>-1</sup>	Total pore volume/mm <sup>3</sup> g <sup>-1</sup>
PS-600	2.77	7.82
PS-750	41.02	14.65
PS-900	4.14	6.48

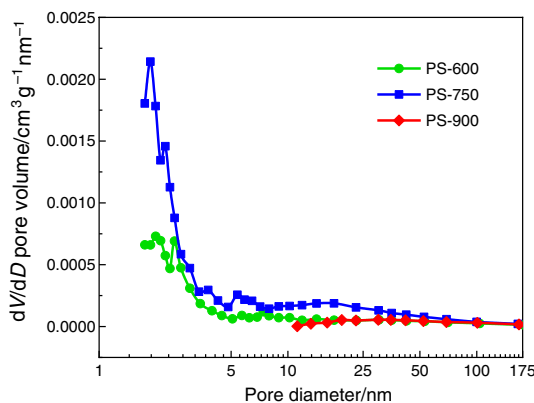


**Fig. 6** Pore-size distribution of semi-coke

while the char itself can also act as a type of reducing agent for the NO reduction reaction. Thus, the morphological properties of semi-coke were investigated using a surface area and pore-size distribution analyzer (Micromeritics, ASAP2010). The results of the BET surface area and total pore volume are listed in Table 6. BET surface area was a specific surface area calculated following the well-known BET theory. Total pore volume was BJH adsorption cumulative volume of pores, whose the pore diameter was between 1.7 and 300 nm.

It was suggested that the specific surface area and pore volume of the semi-coke increased first and then decreased while the pyrolysis temperature increased. The change process of the pore structure during pyrolysis could not be obtained relying on the above data. In order to explore the change process of the pore structure, the pore-size distributions of semi-coke were calculated by the classic BJH model [36]. In addition, the pore-size distributions are shown in Fig. 6.



During the pyrolysis, the moisture and volatile would release gradually. With the pyrolysis temperature increasing, the precipitation of volatiles and moisture would be more complete. Thermally unstable components were gradually lost, and the carbon skeleton was more and more clear. Hence, PS-750 had more micropores and mesopores than PS-600. However, when the pyrolysis temperature increased from 750 to 900 °C, plastic deformation of complex pore structure and collapse of carbon skeleton happened for the existence of thermal stress. Besides, some of the minerals with lower ash melting points began to melt, and the molten minerals blocked some of the micropores. The micropores gradually disappeared for the above reasons. This resulted in a decrease in specific surface area and porosity. Thus, PS-750 had the most developed pore structure.

## TG–MS experiment

### Combustion reaction kinetic analysis of samples

The TG/DTG curves of the samples under the combustion conditions are shown in Fig. 7. In this study, the TG–DTG method was employed to determine ignition temperature, maximum mass loss temperature and burnout temperature. A vertical line was made over the peak point on the DTG curve. Subsequently, a tangent line was made at the intersection of the vertical line and the TG curve. The temperature corresponding to the intersection of the tangent line and the mass loss starting parallel line was defined as the ignition temperature ( $T_i$ ). Likewise, the burnout temperature ( $T_b$ ) was the temperature corresponding to the intersection of the tangent line and the mass loss ending parallel line. The temperature corresponding to the peak point of DTG was the maximum mass loss temperature ( $T_{max}$ ) [37].

There was no mass loss peak in DTG curves at around 100 °C like other coals, because there was almost no moisture in PS and its semi-cokes. The difference of total mass

loss between the PS and semi-coke was caused by different content of ash. It was noteworthy that there were mass loss peaks at around 700 °C in PS and PS-600, and this second mass loss peak did not appear in PS-750 and PS-900. This mass loss peak must be caused by the decomposition of  $\text{CaCO}_3$  in ash. The total mass loss of PS was approximately 55%, whereas the ash composition ratio of PS was 55%, it means that  $\text{CaCO}_3$  decomposed in the course of combustion.

With the rise in the pyrolysis temperature,  $T_i$ ,  $T_b$  and  $T_{max}$  of samples, listed in Table 7, increased. There were three reasons resulting in that high temperature pyrolysis semi-coke was difficult to ignite than low temperature pyrolysis semi-coke. Firstly, the content of volatiles decreased with the pyrolysis temperature increasing. Moreover, the degree of graphitization for semi-coke also increased with increasing temperature. Furthermore, the proportion of ash became larger when the pyrolysis temperature increased. The presence of minerals hindered the heat conduction and diffusion of  $\text{O}_2$ . The larger ash proportion meant the larger resistance of heat and mass transfer. Hence, the ignite characteristics of semi-coke gradually worsened with increasing pyrolysis temperature.

Table 7 also lists  $(dm/dt)_{mean}$ , which represents the average mass change rate during the whole experiment. The calculation formula is as follows:

$$\left(\frac{dm}{dt}\right)_{mean} = \frac{100 - m_f}{t} \quad (4)$$

The  $m_f/\%$  was the remaining mass ratio after combustion reaction and  $t/\text{min}$  was the whole reaction time.

It can be seen that the average mass loss rate of PS was higher than its semi-coke. The  $(dm/dt)_{mean}$  decreased significantly after pyrolysis. Nevertheless,  $(dm/dt)_{mean}$  between three kinds of semi-coke had no obvious difference. Pyrolysis temperature had little influence on the average mass loss rate of semi-coke. Increasing the pyrolysis temperature was more like making the whole combustion reaction process to high temperature region. In other words, increasing the pyrolysis temperature only worsened the ignition characteristics, but almost had no influence on the burnout of semi-coke. On the one hand, a well-developed pore structure of semi-coke ensured stable

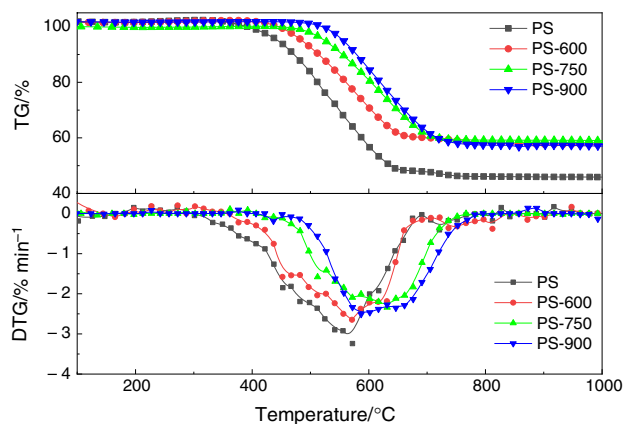


Fig. 7 TG/DTG curves of PS and its semi-cokes

Table 7 Combustion characteristic parameter of samples

Sample	$T_i/^\circ\text{C}$	$T_{max}/^\circ\text{C}$	$T_b/^\circ\text{C}$	$(dm/dt)_{mean}/\% \text{ min}^{-1}$
PS	360.1	572	646.8	-0.0394
PS-600	385.7	583.2	662.5	-0.0308
PS-750	480.1	618.7	714.1	-0.0295
PS-900	510.8	656.3	738.3	-0.0318

combustion after ignition. On the other hand, the high temperature exacerbated combustion reaction.

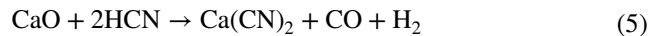
### Release characteristics of gaseous products in samples combustion

Under combustion conditions of coal, nitrogen-containing gaseous products include HCN, NH<sub>3</sub>, NO, NO<sub>2</sub> and N<sub>2</sub>O. The release rates of all gaseous products with a molecular mass between 0 and 64 could be quantitatively calculated by ECSA [30–32]. ECSA was a novel method to analyze the mass spectrum and giving the mass flow rate of all evolved gases as precise as possible based on the operating principle of the TG–MS coupling system. As a result, this method could separate the mass spectrum, eliminated the mass discrimination and temperature-dependent effect, even if there were some overlaps at the characteristic peak. After calculation, the release rates of the above-mentioned gaseous pollution were in the same magnitude with interference signal except HCN and NO. The release curves of main gaseous products (e.g., CO<sub>2</sub>, HCN and NO) are shown in Fig. 8.

The release rate of CO<sub>2</sub> reflected the intensity of the combustion reaction. It was clear that the CO<sub>2</sub> starting releasing temperature of PS was lower than semi-cokes. The temperature at which CO<sub>2</sub> began to release in semi-cokes increased with the rise in the pyrolysis temperature. The CO<sub>2</sub> release curves of PS and PS-600 had two peaks while there was only one peak in CO<sub>2</sub> release curves of PS-750 and PS-900. The first peak was caused by lots of CO<sub>2</sub> released from the

combustion reaction. The second CO<sub>2</sub> release peak was caused by the decomposition of CaCO<sub>3</sub>.

Nitrogen-containing gaseous pollutants were mainly NO and HCN. Normally, the gaseous precursors of NO were HCN and NH<sub>3</sub> [38]. However, the yield of HCN in this study was much larger than that of NH<sub>3</sub>, thus NH<sub>3</sub> could be negligible. The yields of HCN for PS-750 and PS-900 were lower than PS-600. It was because the presence of CaO promoted the hydrolysis of HCN by following reaction [39]. That was the reason why there was less HCN released during the combustion of PS-750 and PS-900.



The smallest maximum release rates of the four samples were  $2.29 \times 10^{-3} \text{ mg min}^{-1}$  for PS-750 owing to the most developed pore structure of PS-750. Developed pore structure prolongs the time for diffusion of HCN from the interior to the surface of the char particle. Hence, HCN would be more easily hydrolyzed by the above reaction.

The starting releasing temperature of NO was increased with the pyrolysis temperature increased. This was because, during the pyrolysis process, relatively unstable nitrogen morphology had transformed into pyrolysis gas or more stable nitrogen morphology with higher combining energy. During the combustion, the nitrogen binding energy in the semi-coke was higher, the stability was stronger, and the release was more difficult.

The maximum NO release rate of PS reached  $0.0141 \text{ mg min}^{-1}$  when the combustion temperature was 620 °C. Similar to PS, the maximum NO release rate of PS-600 was  $0.0138 \text{ mg min}^{-1}$  at 628 °C. However, the maximum NO release rate of PS-750 and PS-900 was  $0.0104 \text{ mg min}^{-1}$  and  $0.0091 \text{ mg min}^{-1}$ , respectively, when the temperature was around 673 °C. On the one hand, the total nitrogen content was considered the most important factor affecting the NO emission concentration. Higher nitrogen content could result in higher NO emission. On the other hand, the change of ash compounds could not be ignored. There was no discussion about the effect of alkali metal due to almost the same content in samples. But the content of Ca in PS-900 was lower than PS-750, the formation of Ca(CN)<sub>2</sub> preferentially direct the conversion of fuel-N toward NO during coal combustion [11]. For the above reasons, the yield of NO decreased with the rise in the pyrolysis temperature.

In this work, the released HCN would be taken away by the carrier gas quickly. Therefore, the influence of HCN on the NO<sub>x</sub> emission did not reflect. However, there were two main conversion routes in the actual boiler [38, 40]. One was the oxidation of HCN via NCO to NO<sub>x</sub>. Moreover, HCN was hydrolyzed and converted into NH<sub>3</sub>. Then, NH<sub>3</sub> by hydrolysis not only led to an additional formation of NO at medium

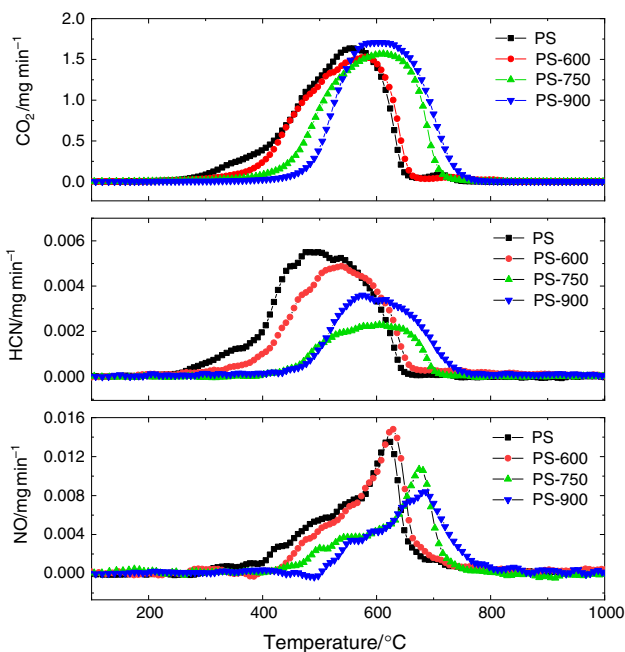


Fig. 8 The release curves of main gaseous products

**Table 8** The total release amount of main gaseous product

Sample	CO <sub>2</sub> /mg	HCN/mg	NO/mg	$\omega/\%$
PS-600	28.826	0.098	0.169	63.6
PS-750	30.583	0.043	0.123	40.3
PS-900	31.169	0.070	0.118	49.1

temperatures but also to an additional decomposition of NO at elevated temperatures.

The area under the release curves of gaseous products represented the total released mass. The total released mass is obtained by the following formula, and it is exhibited in Table 8.

$$M = \int \left( \frac{dm}{dt} \right)_{\text{release}} dt = \sum \left( \frac{dm}{dt} \right)_{\text{release}} \times 0.1 \quad (6)$$

$M$  was the total released mass.  $(dm/dt)_{\text{release}}$  was the release rate of the gas product. The time interval was 0.1 min, and hence, the equation could be changed to the rightmost form.

Besides, in order to exclude the effect of nitrogen content, the following formula was used to calculate the conversion rate of fuel-N to nitrogen-containing gaseous products (NO and HCN).

$$\omega = \frac{\frac{m_{\text{NO}}}{M_r(\text{NO})} + \frac{m_{\text{HCN}}}{M_r(\text{HCN})}}{m_s \times N_{\text{ar}}} \times A_r(N) \quad (7)$$

The  $m_{\text{NO}}/\text{g}$ ,  $m_{\text{HCN}}/\text{g}$  and  $m_s/\text{g}$  represented the total quality of released NO, HCN and samples, respectively.  $A_r$  and  $M_r$  were the relative atomic mass and relative molecular mass.  $N_{\text{ar}}/\%$  was the content of nitrogen in the sample.

The conversion rate of PS-750 was the lowest due to its most developed pore structure. On the one hand, a more developed pore structure meant a longer time for gas diffusion from inferior to surface. The longer residence time was helpful for the reduction reaction process. On the other hand, the developed pore structure enhanced the catalysis surface of the reduction of NO. Therefore, the reduction reaction of NO was also promoted. Besides, CaO was characterized by better mobility and higher reactivity, which has a greater effect on N<sub>2</sub> formation. Based on the above reasons, the PS-750 had the lowest conversion rate of fuel-N to nitrogen-containing gas.

## Conclusions

The emission of NO and its precursor, HCN, over semi-coke with three different pyrolysis temperatures during combustion was investigated in a TG-MS system. The effect of

pyrolysis temperature on the conversion rates of NO was also explored in this work. Conclusions can be drawn as follows:

- (1) The nitrogen content in semi-coke gradually decreased with increasing pyrolysis temperature while the morphology of nitrogen also changed. N-X and X-6 transform to N-Q rapidly when the pyrolysis temperature exceeded 750 °C owing to the thermal stability of N-Q.
- (2) CaO produced by the decomposition of CaCO<sub>3</sub> would appear in PS-750 and PS-900. The presence of CaO would promote the conversion from HCN to NO.
- (3) There was an optimum pyrolysis temperature to maximize the specific surface area and pore volume of the semi-coke. Developed pore structure was beneficial to the conversion of HCN and reduction of NO.
- (4) The ignition characteristic of semi-cokes worsened with the pyrolysis temperature increasing. However, the burnout of semi-coke was not influenced by the pyrolysis temperature. Namely, the combustion reaction process moved to a high temperature zone with increasing pyrolysis temperature.
- (5) The yield of HCN during combustion first decreased and then increased while the pyrolysis temperature increased. Nevertheless, the yield of NO decreased with the pyrolysis temperature increasing. Hence, there was an optimum pyrolysis temperature for the minimum conversion rate of fuel-N to NO and HCN. For Pingshuo bituminous, the optimum pyrolysis temperature was 750 °C.

**Acknowledgements** This work was financially supported by the National Key Research & Development Program of China, Grant No. 2018YFB0605002 and “Transformational Technologies for Clean Energy and Demonstration,” Strategic Priority Research Program of the Chinese Academy of Sciences, Grant No. XDA21040100.

## References

1. National Bureau of Statistics of the People's Republic of China. China statistical yearbook. Beijing: China Statistics Press; 2018.
2. Cen K. Research progress and outlook for efficient, clean and low-carbon coal utilization. *Sci Technol Rev.* 2018;36(10):66–74.
3. Xu M, Li S, Wu Y, et al. Reduction of recycled NO over char during oxy-fuel fluidized bed combustion: effects of operating parameters. *Appl Energy.* 2017;199:310–22.
4. Xu M, Li S, Wu Y. The characteristics of recycled NO reduction over char during oxy-fuel fluidized bed combustion. *Appl Energy.* 2017;190:553–62.
5. Johnsson JE. Formation and reduction of nitrogen oxides in fluidized-bed combustion. *Fuel.* 1994;73:1398–415.
6. Furusawa T, Tsunoda M, Tsujimura M, et al. Nitric oxide reduction by char and carbon monoxide: fundamental kinetics of nitric oxide reduction in fluidized bed combustion of coal. *Fuel.* 1985;64(9):1306–9.



7. SchönNenbeck C, Gadiou R, Schwartz D. A kinetic study of the high temperature NO-char reaction. *Fuel*. 2004;83(4-5):443-50.
8. Wu X, Song Q, Zhao H, et al. Kinetic modeling of inherent mineral catalyzed NO reduction by biomass char. *Environ Sci Technol*. 2014;48(7):4184-90.
9. Wang Q, Liu Y, Xu F, et al. Insights on structural characteristic of Xilinguole lignite chars from low-temperature pyrolysis. *J Therm Anal Calorim*. 2019;136:1631-43.
10. Sun S, Zhang J, Hu X, et al. Studies of NO-char reaction kinetics obtained from drop-tube furnace and thermogravimetric experiments. *Energy Fuels*. 2009;23:74-80.
11. Zhao Z, Li W, Qiu J, et al. Influence of Na and Ca on the emission of NO<sub>x</sub> during coal combustion. *Fuel*. 2006;85(5-6):601-6.
12. Ralf FW, Halang S. Catalytic influence of ash elements on NO<sub>2</sub> formation in char combustion under fluidized bed conditions. *Fuel*. 1997;76(4):345-51.
13. Patsias AA, Nimmo W, Gibbs BM. Calcium-based sorbents for simultaneous NO<sub>x</sub>/SO<sub>x</sub> reduction in a down-fired furnace. *Fuel*. 2005;84(14-15):1864-73.
14. Qin Y, He Y, Ren W, et al. Catalytic effect of alkali metal in biomass ash on the gasification of coal char in CO<sub>2</sub>. *J Therm Anal Calorim*. 2020;139:3079-89.
15. Wang C, Zhao L, Yuan M, et al. Effects of minerals containing sodium, calcium, and iron on oxy-fuel combustion reactivity and kinetics of Zhundong coal via synthetic coal. *J Therm Anal Calorim*. 2020;139:261-71.
16. Zhao B, Jin J, Li S, et al. Co-pyrolysis characteristics of sludge mixed with Zhundong coal and sulphur contaminant release regularity. *J Therm Anal Calorim*. 2019;138:1623-32.
17. Ren Q, Zhao C, Wu X, et al. Catalytic effects of Fe, Al and Si on the formation of NO<sub>x</sub> precursors and HCl during straw pyrolysis. *J Therm Anal Calorim*. 2010;99(1):301-6.
18. Solomon PR, Fletcher TH, Pugmire RJ. Progress in coal pyrolysis. *Fuel*. 1993;72(5):587-97.
19. Hou J, Ma Y, Li S, et al. Transformation of sulfur and nitrogen during Shenmu coal pyrolysis. *Fuel*. 2018;231:134-44.
20. Tian F, Li B, Chen Y, et al. Formation of NO<sub>x</sub> precursors during the pyrolysis of coal and biomass. Part V. Pyrolysis of a sewage sludge. *Fuel*. 2002;81(17):2203-8.
21. Guo L, Zuo H, Wang Y, et al. Thermal behavior and kinetic study on the pyrolysis of lean coal blends with thermally dissolved coal. *J Therm Anal Calorim*. 2019;136:903-12.
22. Wu D, Zhang W, Fu B, et al. Chemical structure and gas products of different rank coals during pyrolysis. *J Therm Anal Calorim*. 2019;136:2017-23.
23. Thomas KM. The release of nitrogen oxides during char combustion. *Fuel*. 1997;6(6):457-73.
24. Hayhurst AN, Lawrence AD. The amounts of NO<sub>x</sub> and N<sub>2</sub>O formed in a fluidized bed combustor during the burning of coal volatiles and also of char. *Combust Flame*. 1996;105(3):341-57.
25. Ren Q. NO<sub>x</sub> and N<sub>2</sub>O precursors from co-pyrolysis of biomass and sludge. *J Therm Anal Calorim*. 2013;112(2):997-1002.
26. Ren Q. NO<sub>x</sub> and N<sub>2</sub>O precursors from biomass pyrolysis. *J Therm Anal Calorim*. 2014;115(1):881-5.
27. Yang Y, Lu X, Wang Q. Investigation on the co-combustion of low calorific oil shale and its semi-coke by using thermogravimetric analysis. *Energy Convers Manag*. 2017;136:99-107.
28. Liu H, Gong S, Jia C, et al. TG-FTIR analysis of co-combustion characteristics of oil shale semi-coke and corn straw. *J Therm Anal Calorim*. 2017;127(3):2531-44.
29. Hu L, Zhang Y, Chen D, et al. Experimental study on the combustion and NO<sub>x</sub> emission characteristics of a bituminous coal blended with semi-coke. *Appl Therm Eng*. 2019;160:113993.
30. Xia H, Wei K. Equivalent characteristic spectrum analysis in TG-MS system. *Thermochim Acta*. 2015;602:15-21.
31. Huang Q, Wei K, Xia H. A novel perspective of dolomite decomposition: elementary reactions analysis by thermogravimetric mass spectrometry. *Thermochim Acta*. 2019;676:47-51.
32. Lin Y, Huang Q, Wei K, et al. Quantitative study on adsorption and regeneration characteristics of activated coke using equivalent characteristic spectrum analysis. *Ind Eng Chem Res*. 2019;58(12):5080-6.
33. Marek AW, Pels JR, Moulijn JA. The fate of nitrogen functionalities in coal during pyrolysis and combustion. *Fuel*. 1995;74(4):507-16.
34. Gong B, Buckley AN, Lamb RN, et al. XPS determination of the forms of nitrogen in coal pyrolysis chars. *Surf Interface Anal*. 1999;28(1):126-30.
35. Wang Q, Jiao G, Liu H, et al. Variation of the pore structure during microwave pyrolysis of oil shale. *Oil Shale*. 2010;27(2):135-46.
36. Groen JC, Peffer L, Javier PR. Pore size determination in modified micro- and mesoporous materials. Pitfalls and limitations in gas adsorption data analysis. *Microporous Mesoporous Mater*. 2003;60(1-3):1-17.
37. Yu Q, Pang Y, Chen H. Determination of ignition points in coal-combustion tests. *North China Electric Power*. 2001;7:9-10.
38. Schafer S, Bonn B. Hydrolysis of HCN as an important step in nitrogen oxide formation in fluidised combustion. Part I. Homogeneous reactions. *Fuel*. 2000;79(10):1239-46.
39. Schafer S, Bonn B. Hydrolysis of HCN as an important step in nitrogen oxide formation in fluidised combustion. Part II: heterogeneous reactions involving limestone. *Fuel*. 2002;81(13):1641-6.
40. Ke X, Cai R, Yang H, et al. Formation and ultra-low emission of NO<sub>x</sub> for circulating fluidized bed combustion. *Proc CSEE*. 2018;38(2):390-6.

**Publisher's Note** Springer Nature remains neutral with regard to jurisdictional claims in published maps and institutional affiliations.